Applied Catalysis B: Environmental 168-169 (2015) 141–155

Contents lists available at ScienceDirect

Applied Catalysis B: Environmental

journal homepage: www.elsevier.com/locate/apcatb

Catalytic total oxidation of 1,2-dichloroethane over highly dispersed vanadia supported on CeO_2 nanobelts

Qiguang Dai[a,*], Shuxing Bai[a], Hua Li[b], Wei Liu[b], Xingyi Wang[a,*], Guanzhong Lu[a]

[a] Key Laboratory for Advanced Materials, Research Institute of Industrial Catalysis, East China University of Science and Technology, Shanghai 200237, PR China

[b] Key Laboratory of Nuclear Radiation and Nuclear Energy Technology, Shanghai Institute of Applied Physics, Chinese Academy of Science, Shanghai 201800, PR China

ARTICLE INFO

Article history:
Received 4 September 2014
Received in revised form
11 December 2014
Accepted 13 December 2014
Available online 24 December 2014

Keywords:
1,2-Dichloroethane
Total oxidation
Vanadia
CeO_2
Reaction mechanism

ABSTRACT

CeO_2 nanobelts were synthesized via a facile aqueous-phase precipitation route under mild conditions (template-free and non-hydrothermal), and then the highly dispersed vanadia catalysts with a wide range of VO_x loadings were prepared by a conventional incipient-wetness impregnation method. The target VO_x/CeO_2 catalysts were characterized in detail and used in catalytic combustion of 1,2-dichloroethane (DCE). The results revealed that the monolayer dispersed VO_x (6.0%VO_x/CeO_2) exhibited the most outstanding initial and stable activities, however, the main product containing carbon was CO, not desired CO_2. A reaction mechanism of DCE total oxidation was proposed based on the study of TPSR and in situ FTIR. The first step of this mechanism was considered to be a dissociative adsorption of C—Cl bonds on Lewis acid sites (such as $Ce^{4+/3+}$, $V^{5+/4+}$ or Ce^{3+}–O^{2-}–V^{5+}) via Cl abstraction, and then the dissociated DCE can be oxidized directly to CO_2 by surface active oxygen species over pure CeO_2. Whereas, over VO_x/CeO_2 catalysts, the formation of intermediate acetaldehyde was a key step via C—H bond activation and hydrogen transfer on VO_x species, subsequently, partially oxidized to CO by the lattice oxygen of VO_x.

1. Introduction

In recent years, high concerns have been raised about atmospheric emission from domestic or industrial exhausts [1,2]. In particular, the release of chlorinated volatile organic compounds (CVOCs) has received much attention due to the major health problems associated with the exposure to these compounds. Several methods have been applied to solve the problem of CVOCs release, including, adsorption/absorption, thermal incineration, catalytic combustion/total oxidation, photocatalytic degradation, steam reforming, hydrodechlorination and biological process, etc. Among these, the catalytic oxidation to CO_x, H_2O, HCl and Cl_2 is the most promising solution due to its low operation temperature, high efficiency and its excellent selectivity towards the formation of harmless products.

Various catalytic materials have been evaluated as catalysts for total oxidation of CVOCs, mainly including noble metals, perovskites, solid acid (such as H-type zeolite) and transition metal oxides based catalysts [3]. Comprehensively considering, transition metal oxide based catalysts appear to be the best candidate. Because, they can convert CVOCs to harmless products at temperature as low as 250 °C, do not produce polychlorinated compounds and prevent the de novo formation of dioxins. Significant investigations pointed out that V_2O_5/TiO_2-based catalysts, which were commercially employed for the reduction of NO_x via NH_3-SCR, also exhibited the outstanding performances for catalytic abatement of chlorinated aromatic hydrocarbons and more resistant to chlorine poisoning. Amiridis [4,5] investigated the oxidation of different chlorinated benzenes (i.e., chlorobenzene, 1,2- 1,3-, and 1,4-dichlorobenzene) and *o*/*p*-chlorophenol over the 3.6wt% V_2O_5/TiO_2 catalyst via kinetic and in situ IR studies, and found out that this catalyst was very active for the oxidation of these (chloro)-aromatic pollutants. Moreover, the authors studied the addition of water during the oxidation of *m*-dichlorobenzene, and the results showed that surface activation was assisted by water through Cl (reverse Deacon reaction) and C (hydrolysis) removal in the low temperature region (<270 °C), hence, a promoting effect was observed. In the high temperature region (>350 °C) water still interacted with and adsorbed on the active vanadia sites, whereas other inhibiting species, such as Cl and C, were no longer retained

* Corresponding authors. Tel.: +86 21 64253183; fax: +86 21 64253372.
E-mail addresses: daiqg@ecust.edu.cn (Q. Dai), wangxy@ecust.edu.cn (X. Wang).

http://dx.doi.org/10.1016/j.apcatb.2014.12.028
0926-3373/

on the catalyst surface leading to an overall deactivating effect [6]. Recently, a large number of fundamental works [7–14] indicated that the addition of a second transition metal oxide (i.e. WO_3, MoO_3) to the V_2O_5–TiO_2 system further improved the performance of vanadia based catalysts in the total oxidation of chlorobenzene or other chlorinated aromatics, such as higher catalytic activity, resistance to poisoning by SO_2 or HCl and improved thermal stability, due to the increase of Brönsted acidity and Lewis acidity. However, the presence of Brönsted acid sites would lead to the uncompleted degradation of chlorinated compounds, promoting the formation of partial oxidation products, as chloromaleic anhydride. On the contrary, Lewis acid sites, acting as absorbing sites, promoted the further oxidation of intermediates to CO and CO_2, without any by-products desorption [12]. Debecker et al. [13] reported that the adding of silica to $V_2O_5/WO_3/TiO_2$ further improved its catalytic performance, which favored the formation of highly dispersed VO_x species and leaded to a stabilization of the catalyst. These studies clearly confirm the VO_x supported on TiO_2 catalysts as the most performing, stable and most promising formulation for the total oxidation of CVOCs. The enhanced activity of supported vanadia was generally considered to result from an interaction between the support and the vanadium oxide at the interface, and the catalytic activity of supported vanadium oxide catalysts was significantly affected by the properties of the supports. However, few authors [15–17] reported the effects of other supports except TiO_2 on the catalytic oxidation of CVOCs over VO_x based catalysts, and few non-chlorinated aromatic compounds were investigated [18]. In practice, the 1,2-dichloroethane (DCE) and vinyl chloride (VC) are probably the most important CVOCs emitted from waste streams in chemical plants, as they are widely employed in the production of polyvinyl chloride (PVC), as a solvent in textile cleaning, degreasing of metal parts, dispersant of plastics and elastomers and as a chemical agent in formulations of paints and enamels. Therefore, the catalytic oxidation of DCE or VC is significant over VO_x supported on non-TiO_2 carrier catalysts. Over the past several years, CeO_2 and CeO_2-containing catalysts [17,19–22] have attracted much attention in the field of CVOCs oxidation, due to a rapid and reversible Ce^{4+}/Ce^{3+} redox cycles at moderate temperature and high catalytic activity. However, the strong adsorption of HCl or Cl_2 on the active sites results in the rapid deactivation of CeO_2 catalysts. Given VO_x based catalysts demonstrate an outstanding resistance to poisoning by HCl, so there is a reason to speculate that VO_x/CeO_2 catalysts display different catalytic behavior for the total oxidation of CVOCs.

In this study, we report the preparation of VO_x/CeO_2 catalysts with high dispersion and VO_x loadings by employing CeO_2 nanobelts as the support. The dispersibility, the redox properties and surface acidity/basicity of VO_x supported on CeO_2 nanobelts, and the total oxidation of DCE are investigated. The oxidation of DCE, including activity, stability, product distribution, and water effects, is studied in detail. Moreover, the reaction pathway is explored via in situ FTIR studies.

2. Experimental

2.1. Synthesis of CeO_2 nanobelts

In a typical synthesis procedure, 1.39 g cerium(III) nitrate hexahydrate ($Ce(NO_3)_3{\cdot}6H_2O$) and 0.75 g ammonium bicarbonate (NH_4HCO_3) were dissolved in 200 ml and 25 °C deionized water under magnetic stirring, respectively. After completely dissolved, the NH_4HCO_3 solution was poured rapidly into the $Ce(NO_3)_3$ solution, and then stirring for 0.5 h and statically aging 15 h at 25 °C. The final product was collected by filtration, washed with deionized water, and then dried at 80 °C and calcined at 450 °C for 4 h in air. The specific surface area (BET method) of synthesized CeO_2 nanobelts, with a thickness of about 20–50 nm, a length of about 5–10 μm and a width of about 0.5–1.2 μm, was 86 cm^3/g. The more detailed procedures and characterizations can be found in Reference [23].

2.2. Preparation of supported vanadia catalysts

Vanadia was deposited on the ceria support using incipient wetness of an aqueous solution of ammonium metavanadate (NH_4VO_3) and oxalic acid ($C_2O_4H_2$) in a 1:2 molar ratio. The concentration of vanadate and the amount of impregnation solution was adjusted in order to produce catalysts with 1.25–10 wt% vanadia weight loadings (calculated by V_2O_5). After impregnation of the vanadate, the samples were dried overnight at 60 °C and then calcined in air at 450 °C for 4 h. The obtained catalysts were marked as $m\%VO_x/CeO_2$ (m = 1.25, 2.5, 5.0, 6.0, 6.5, 7.0, 7.5 and 10), and the real V loadings measured by ICP-AES analysis were 0.7, 1.1, 2.1, 2.5, 2.8, 2.9, 3.2 and 4.1, respectively.

The bulk VO_x catalyst was obtained by calcining NH_4VO_3 in air at 450 °C for 4 h.

2.3. Catalysts characterization

The powder X-ray diffraction patterns (XRD) of samples were recorded on a Rigaku D/Max-rC powder diffractometer using Cu Ka radiation (40 kV and 100 mA). The real V_2O_5 loadings were measured by ICP-AES analysis on Thermo Elemental IRIS 1000. The nitrogen adsorption and desorption isotherms were measured at 77 K on an ASAP 2400 system in static measurement mode. The samples were outgassed at 160 °C for 4 h before the measurement. The specific surface area was calculated using the BET model. The Raman spectra were obtained on a Renishaw in Viat + Reflex spectrometer equipped with a CCD detector at ambient temperature. The emission line at 514.5 nm from an Ar^+ ion laser (Spectra Physics) was focused, analyzing spot about 1 mm, on the sample under the microscope. FTIR absorption spectra of catalysts powders are measured by KBr disk method over the range 4000–400 cm^{-1} on Nicolet 6700 spectrometer. High resolution TEM (HRTEM) images were recorded on a JEM-2100 instrument operated at 200 kV. Scanning electron microscopy (SEM) experiments were performed on Hitachi S-3400N electron microscopes. ESR measurements have been performed on a BRUKER EMX-8/2.7C X-band spectrometer with 100 kHz modulation at room temperature. The microwave frequency was 9.880 GHz. The XPS measurements were made on a VG ESCALAB MK II spectrometer by using Mg Kα (1253.6 eV) radiation as the excitation source. Charging of samples was corrected by setting the binding energy of adventitious carbon (C1 s) at 284.6 eV.

Hydrogen temperature programmed reduction (H_2-TPR) was performed in a U-type tube quartz reactor using a TCD as detector. 100 mg sample was used and heated in O_2 at 450 °C for 1 h. Then the sample was cooled to 100 °C in O_2 flow (30 ml/min). The reducing gas was 5 vol.% H_2/Ar and its flow rate was 30 ml/min. The sample was heated at 10 °C/min from 100 to 750 °C.

The temperature-programmed desorption of NH_3 (NH_3-TPD) and CO_2 (CO_2-TPD) was carried in the same equipment (a U-type tube quartz reactor) and the effluent was monitored by a TCD and Hiden HPR20 MS, respectively. Prior to adsorption experiments, 100 mg of catalyst were pretreated for 1 h at 200 °C in an argon flow with a flow rate of 30 ml/min. Upon cooling to 100 °C, the samples were saturated with a pure NH_3 or CO_2 flow, and then the physisorbed NH_3 or CO_2 were removed through purging with argon gas for 30 min. The samples were then heated to 500 °C at a heating rate of 10 °C/min in argon under a flow rate of 30 ml/min.

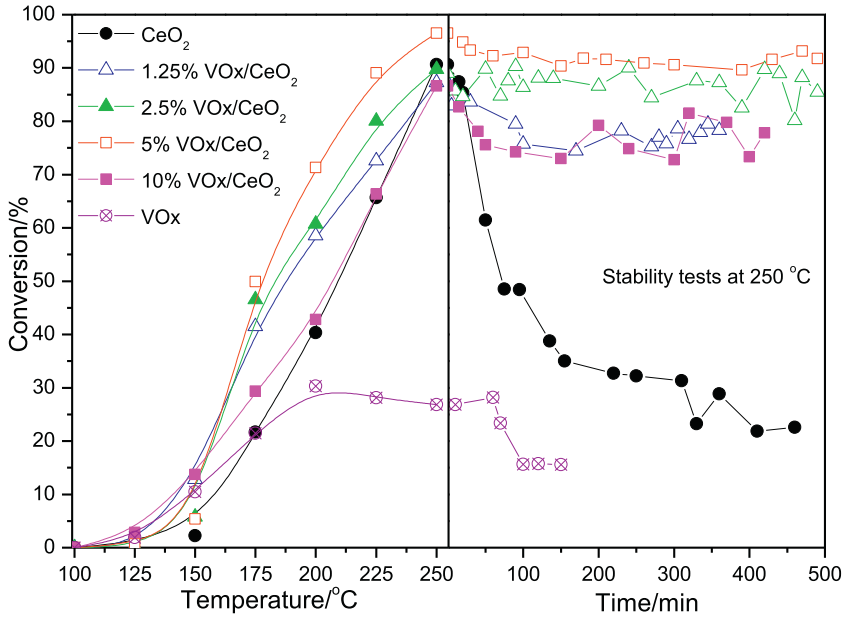

Fig. 1. Light-off curves of 1,2-dichloroethane over VO_x/CeO_2 catalysts with different VO_x loadings, and stability tests of catalysts at 250 °C.

2.4. Catalytic activity measurement

Catalytic oxidation of 1,2-dichloroethane and vinyl chloride was carried out with 200 mg of catalyst (40–60 mesh) in a continuous flow micro-reactor constituted of a U-shaped quartz tube of 3 mm of inner diameter at atmospheric pressure. The gas stream was composed of 450 ppm of DCE or VC and air in 50 ml/min, the space-velocity was 15,000 ml/h·gcat. The reaction was run from 100 to 250 or 300 °C (under 3v/v% H_2O conditions) or 400 °C (for the catalytic combustion of vinyl chloride) in a step mode with a 15 min plateau at each temperature investigated. The effluent gases were analyzed by an on-line gas chromatograph equipped with a flame ionization detector (FID).

The temperature-programmed surface reaction (TPSR) measurements were carried out under the conditions as the same as that in the catalytic activity tests in order to detect the reactants and products in effluence. First, the feeding 20%O_2/Ar stream containing 1000 ppm DCE flowed through the catalyst bed at 100 °C. After the adsorption-desorption of DCE reached an equilibrium, the catalyst bed was heated from 100 to 250 °C at 10 °C/min and maintained for 90 min, and then raised to 300 °C and held for 120 min. Reactants and products in effluence were analyzed on-line by a mass spectrometer apparatus (HIDEN HPR-20).

In situ diffuse reflectance infrared fourier transform (DRIFT) spectroscopy of 1,2-dichloroethane adsorbed on the catalysts was measured on a Nicolet Nexus 6700 spectrometer equipped with a MCT detector and high-temperature sample cell which was fitted with ZnSe windows. The DRIFT spectra obtained were collected in Kubelka–Munk unit with a resolution of 4 cm^{-1} and 64 scans. About 50 mg of catalyst was pre-treated by heating 1 h at vacuum (3.0×10^{-4} mbar) and 200 °C to remove the adsorbed CO_2 and H_2O, and then cooling to 50 °C in a mixture of N_2 and O_2. The spectrum recorded at 50 °C after the thermal treatment was used for substraction as a blank. Next, 100 μl DCE was injected into the cell at 50 °C, and maintained for 15 min. And then, the cell was purged at 50 °C for 30 min under the mixtures of O_2 and N_2 atmosphere to remove the gas phase species. Subsequently, the spectrum was recorded. Afterwards, the sample was heated up to 100 °C and the DCE was again re-introduced into the cell for 30 min. After evacuation with the mixtures of O_2 and N_2 and cooling (50 °C) the spectrum was taken. This experimental procedure was repeated up to 300 °C. In this way, possible transformations of the adsorbed species were recorded at a series of increasing temperatures.

3. Results and discussion

3.1. Catalytic activity and monolayer dispersion of VO_x

Fig. 1 demonstrates light-off curves of 1,2-dichloroethane over VO_x/CeO_2 catalysts with different VO_x loadings and stability tests (at 250 °C). Briefly, a noticeable catalytic activity is observed for the pure CeO_2 and the VO_x supported CeO_2 catalysts, and the 90% conversion of DCE can be achieved at about 250 °C. In contrast, the pure VO_x catalyst displays a poor catalytic activity and reaches only 30% conversion at 250 °C. Moreover, it is found that the VO_x/CeO_2 catalysts exhibit a rising conversion with the increasing of VO_x loadings from 0% to 5%, the 5.0%VO_x/CeO_2 catalyst shows the highest activity and the T_{90} value (the reaction temperature required to reach 90% conversion) is only 230 °C. However, further increasing the VO_x loading to 10%, the VO_x/CeO_2 catalyst shows indeed a declined catalytic activity (T_{90} value is higher than 250 °C) and its light-off curve is similar to that over the pure CeO_2 especially at higher temperature ranges. Our previous works [19] indicated that the deactivation of the catalysts was the most challenging issue for the catalytic combustion of CVOCs over CeO_2 based catalysts, therefore, the stability tests of VO_x/CeO_2 catalysts are carried out at 250 °C. As shown in Fig. 1 right, the obvious deactivation of both pure VO_x and CeO_2 catalysts is observed, by comparison, the conversion of DCE over VO_x/CeO_2 catalysts only presents a slight decrease within the initial 60 min, and then maintained at a constant value within the test duration of 500 min. For examples, the stable conversions over 2.5% and 5.0%VO_x/CeO_2 catalysts are about 85% and 90%, and the 75% conversion also can be achieved over 1.25% and 10%VO_x/CeO_2 catalysts. Obviously, the loading of VO_x improves the catalytic performance of CeO_2 catalyst for the catalytic combustion of DCE, especially the stability. Even low VO_x loading (1.25%) can greatly improve the stability of CeO_2, however, the too high VO_x loading (10%) cannot swell the initial and stable activities further.

XRD patterns of the VO_x/CeO_2 catalysts with different VO_x loadings are recorded and displayed in Fig. 2. All VO_x/CeO_2 catalysts exhibit only the characteristic peaks of the cubic fluorite structure

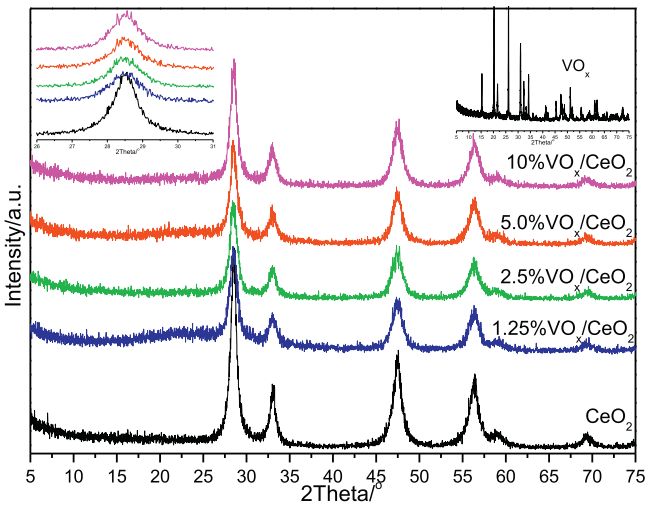

Fig. 2. XRD patterns of the VO_x/CeO_2 catalysts with different VO_x loadings.

of ceria (PDF#34-0394), without any crystalline phase ascribed to VO_x or $CeVO_4$, which suggests that the vanadia species are highly dispersed on CeO_2 surface, or exist in the form of amorphous phase or solid solution. However, the main peak (28.7°) does not shift to low or high degree, which indicates that the VO_x does not distort the CeO_2 crystallization or transfer into the crystal lattice of ceria to form a solid solution. Thereby, the VO_x species likes to only anchor the surface cerium atoms rather than replacing cerium atoms to produce surface defects [24].

Fig. 3 presents the Raman spectra of VO_x/CeO_2 catalysts with different VO_x loadings compared with the spectra for pure CeO_2 and VO_x (Fig. 3inset). The pure CeO_2 shows a strong peak at about 464 cm^{-1}, which is attributed to the Raman-active vibration mode (F_{2g}) of the fluorite – type structure. It can be viewed as a symmetrical stretching vibration of the oxygen anions around cerium ions. Furthermore, the Raman spectra also exhibit other three weak bands at around 252, 590 and 1176 cm^{-1}, which are attributed to the doubly degenerate TO mode, the nondegenerate LO mode and the combination of A_{1g}, E_g and F_{2g} modes [19]. For the VO_x sample prepared by thermal decomposition of NH_4VO_3, the high-frequency Raman peak at 994 cm^{-1} corresponds to the terminal

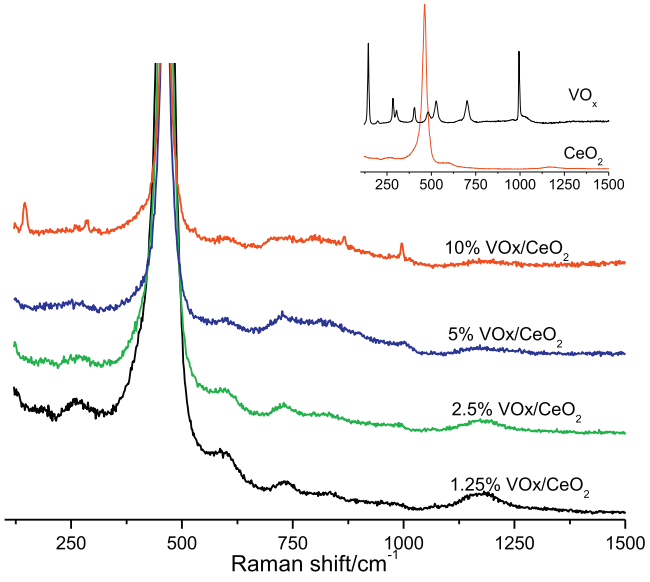

Fig. 3. Raman spectra of the VO_x/CeO_2 catalysts with different VO_x loadings.

oxygen (V=O) stretching mode which results from an unshared oxygen. The peak at 702 cm^{-1} is assigned to the doubly coordinated oxygen (V_2—O) stretching mode and the peak at 529 cm^{-1} is assigned to the triply coordinated oxygen (V_3—O) stretching mode. The two peaks located at 401 and 289 cm^{-1} are assigned to the bending vibration of the V=O bonds. The peaks located at 484 and 308 cm^{-1} are attributed to the bending vibrations of the bridging V—O—V (doubly coordinated oxygen), and the triply coordinated oxygen (V_3—O) bonds, respectively. Other two Raman peaks with low-frequency at 197 and 142 cm^{-1} can be distinguished which correspond to the lattice vibration and strongly associated with the layered structure [25]. For 10%VO_x/CeO_2 catalyst, four sharp bands centered at 149, 285, 868 and 996 cm^{-1} are noted, suggesting the presence of well-defined phase of V_2O_5, however, the corresponding XRD results didn't give any signal attributed to the vanadium oxide. At the same time, no obvious Raman peaks (very weak and broad bands) ascribed to the VO_x species are found for the 1.25 ~ 5% VO_x loadings. Raman is a probe of the influence of even localized short-range order to the vibrational modes of bond configurations, while XRD is well known to probe the long-range order crystallinity of materials [26]. Therefore, the observed phenomenon indicates that the VO_x species on CeO_2 are mainly amorphous and highly dispersed.

Additionally, it is generally recognized that the broad band at around 590 and 1176 cm^{-1}, which have been related to the presence of oxygen vacancies, and the band intensity ratio of 590 and 1176 to 464 cm^{-1}, $(I_{590}+I_{1176})/I_{464}$, suggests the number of the defect sites of ceria-based catalysts. Thus, it can be found that surface defects of catalysts decrease with increasing VO_x loading, indicating that surface VO_x species inhibit the formation of defects (surface oxygen vacancy) on ceria. Vanadium atom could bond to surface by forming V—O—Ce groups, capping oxygen defects and stabilizing the neighboring cerium atoms.

The sharp peak at 670 °C corresponds to the reduction of V_2O_5–V_6O_{13} (α peak), the peak at 710 °C is associated with the reduction of V_6O_{13}–V_2O_4 (β peak), and the peak above 750 °C corresponds to V_2O_3 formed by the reduction of V_2O_4. This reduction of the phenomenon is quiet similar to Kim's work [27]. Compared with the pure VO_x, the main feature of the VO_x/CeO_2 samples is the obvious shift of their reduction peaks to lower temperature region (between 330 °C and 580 °C, and the peak temperature is about 515 °C), as shown in profiles b–e in Fig. 3. The reduction peak at lower temperature region may be assigned to the surface oxygen species from the highly dispersed vanadia on CeO_2 surface, and the peak above 750 °C corresponds to the lattice oxygen from CeO_2, which is comparable to that of pure CeO_2. However, the consumption of hydrogen is increased obviously with the VO_x loading. Meanwhile, further increase of VO_x loadings up to 10 wt.%, the major peak is shifted to higher temperature (about 540 °C), and a new shoulder reduction peak is observed between 600 °C and 680 °C, the new peak can be attributed to the reduction of bulk or multilayer VO_x species on the CeO_2 surface Fig. 4.

The characterization of XRD, Raman and TPR confirms that 1.25 ~ 5% VO_x loadings are below the monolayer dispersion capacity of VO_x species on CeO_2. As well known, the generation of monolayer metal oxides dispersed on the solid supports is very important for the supported metal oxide catalysts, and the optimum catalytic activity of the catalysts is often near its monolayer dispersion capacity likewise the best catalytic performance was obtained at vanadium loadings that gave a vanadium monolayer on the TiO_2 surface [28,29]. Additionally, the catalytic activity tests (Fig. 1) also indicates the performance of VO_x/CeO_2 catalysts is strongly correlated to the VO_x loadings. Therefore, the determination of the dispersion capacity of VO_x supported on CeO_2 is important for optimizing catalysts of DCE catalytic combustion. Subsequently, the VO_x loadings are accurately screened between

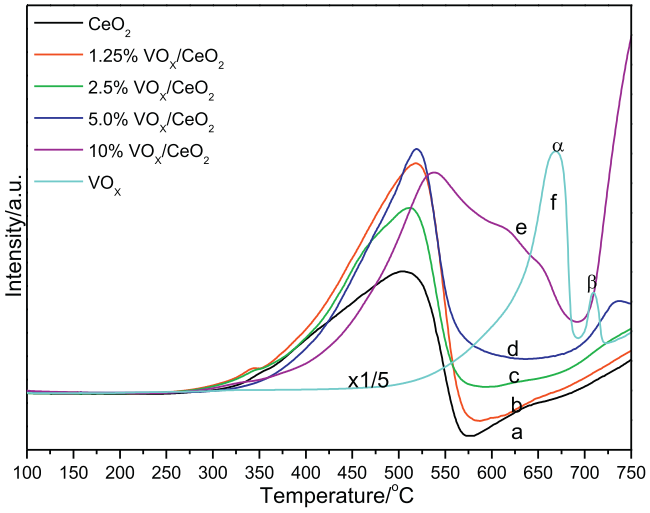

Fig. 4. H_2-TPR profiles of the VO_x/CeO_2 catalysts with different VO_x loadings.

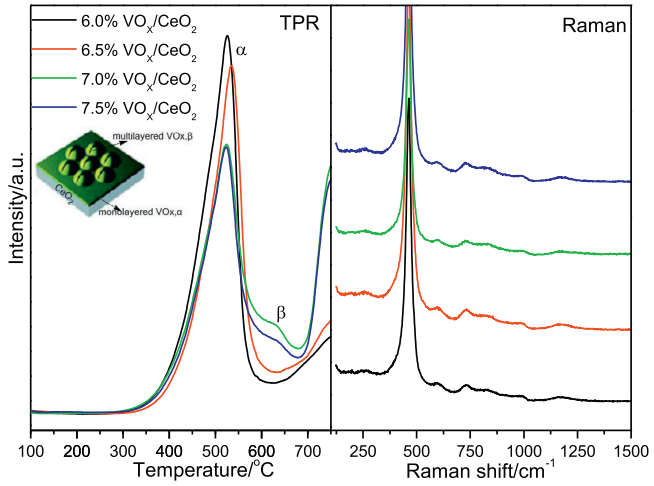

Fig. 5. H2-TPR profiles and Raman spectra of the $VO_x/CeO2$ catalysts with different VO_x loadings.

6% and 7.5% at 0.5% intervals, and TPR, Raman and activity tests are investigated and shown in Figs. 5 and 6 .

As shown in Fig. 5, with the VO_x loadings exceed 7.0%, a new reduction peak (β peak) at 630 °C appeared and the referred peak can be attributed to the reduction of bulk or multilayer VO_x species on the CeO_2 surface as described above. This result demonstrates that the monolayer dispersion capacity of the VO_x species on the CeO_2 nanobelt surface is about 6.0 ~ 6.5%. Additionally, it can be found that the α peak area decreases and the peak area at above 750 °C increases significantly with the increasing of VO_x loading to 6.5%, which is consistent with the increasing of bulk or multilayer VO_x species. However, the characteristic Raman spectra corresponding to V_2O_5 or $CeVO_4$ is still not observed (Fig. 5right), even for the 7.0% and 7.5% VO_x/CeO_2 catalysts.

Light-off curves as shown in Fig. 6 indicate that all catalysts exhibit similar and excellent catalytic activity for catalytic combustion of DCE when compared to pure CeO_2, however, the activity of 7.5%VO_x/CeO_2 exhibits a little decline. The stability tests at 250 °C discover no obvious deactivation, and the stable activities of 6.0%VO_x/CeO_2 and 6.5–7.5%VO_x/CeO_2 catalysts can be maintained at 96% and 90% at least within 6 h, respectively. Evidently, the 6.0%VO_x/CeO_2 catalyst possesses better catalytic performance for the catalytic combustion of DCE, which can be comparable with 5.0%VO_x/CeO_2 catalyst. Considering the results of TPR and activity/stability tests, the monolayer dispersion thresholds of the VO_x species on CeO_2 surface is identified as 6.0%. In what follows, 2.5%VO_x/CeO_2 (the far below monolayer dispersed VO_x), 6.0%VO_x/CeO_2 (the monolayer dispersed VO_x) and 10%VO_x/CeO_2 (the multilayer dispersed VO_x) catalysts as the model of VO_x/CeO_2 are characterized and investigated detailed.

3.2. Comprehensive characterization of VO_x/CeO_2 catalysts

Firstly, IR spectra of VO_x/CeO_2, CeO_2 and VO_x catalysts are obtained to further investigate the dispersion of VO_x species on CeO_2 and presented in Fig. 7. For the bulk VO_x, two bands are observed at 1022 cm^{-1} and 820 cm^{-1}, the former is assigned to the V=O stretching vibration, the other is attributable to the coupled

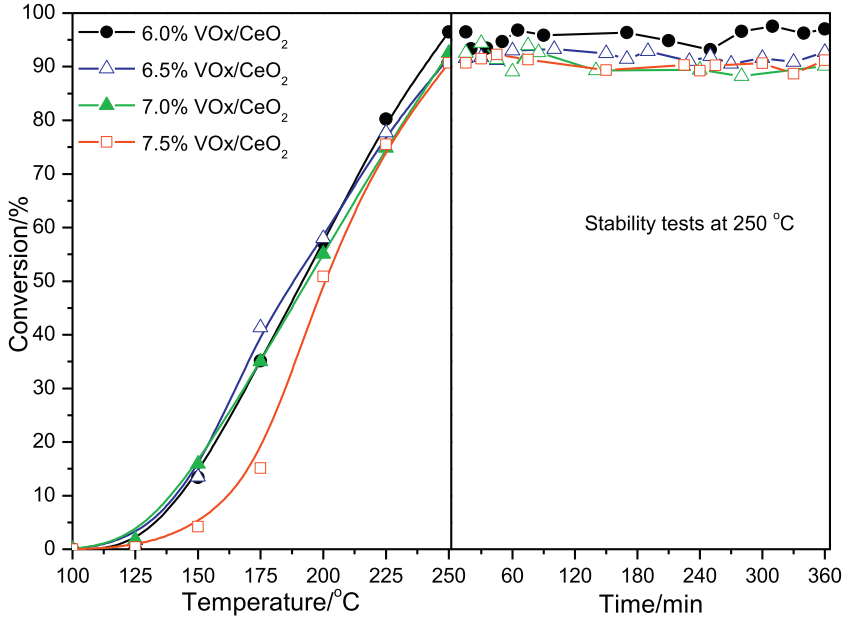

Fig. 6. Light-off curves and stability tests (at 250 °C) of 1,2-dichloroethane over VO_x/CeO_2 catalysts with different VO_x loadings.

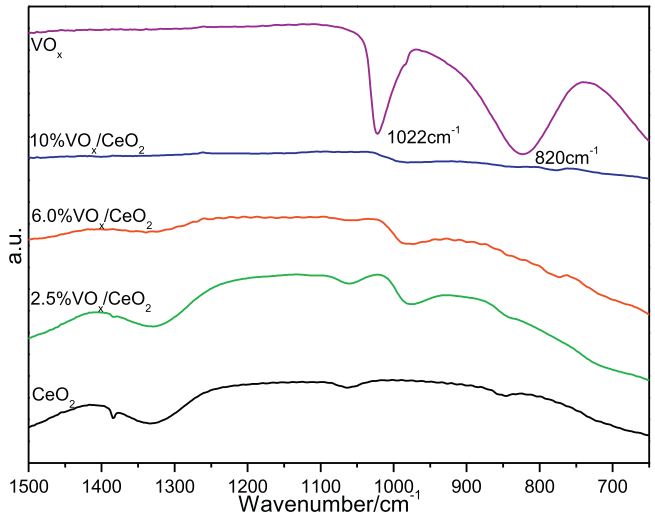

Fig. 7. Infrared spectra of the VO_x/CeO_2 catalysts with different VO_x loadings.

vibration between V=O and to V—O—V. Generally, the crystalline V_2O_5 displays an IR band of V=O at 1020–1025 cm^{-1}, corresponding to the Raman band at 995 cm^{-1}. However, all the VO_x/CeO_2 catalysts give no absorption bands corresponding to crystalline V_2O_5, even the catalyst of $10\%VO_x/CeO_2$ (Raman band at 995 cm^{-1} is observed). This observation suggests that vanadium oxides are highly dispersed, or present amorphous state. Sohn et. al [30] reported that the band at 1022 cm^{-1} was not observed for the V_2O_5–$15WO_3/ZrO_2$ catalysts when vanadium oxide loading was below 18%, due to the high dispersion of V_2O_5 on the surface of zirconia as the amorphous phase. However, increasing the calcination temperature to 800 and 900 °C, the V=O stretching bands due to crystalline V_2O_5 began to appear at 1022 cm^{-1} even for $4V_2O_5$–$15WO_3/ZrO_2$ catalyst. Therefore, the IR results further confirm that the VO_x species highly disperse on the surface of CeO_2 as the formation of the amorphous phase, which is consistent with the Raman and XRD results. Additionally, the BET surface area of the 2.5%, 6.0% and $10\%VO_x/CeO_2$ are 75, 77 and 25 m^2/g, respectively, which shows that the surface area decreases with the addition of VO_x when compared with pure CeO_2 (86 m^2/g), especially for the $10\%VO_x/CeO_2$, thus 10% loadings has been far greater than the monolayer dispersion thresholds of the VO_x species on CeO_2 surface.

Fig. 8 displays HRTEM and SEM images of VO_x/CeO_2 catalysts with different VO_x loadings. The SEM images show that the CeO_2 prepared is mainly consisted of uniform belt-like nanosheets with a length of about 5–10 μm and a width of about 0.5–1.2 μm (Fig. 8a bottom-right), and HRTEM images further display that each nanosheet is composed of numerous densely packed particles with an average size of 3–5 nm. Moreover, the loading of VO_x does not change the morphology of CeO_2 and VO_x/CeO_2 still maintains the belt-like structure (Fig. 8c bottom-right). However, the perceptible VO_x nanoparticles are not observed on all the VO_x/CeO_2 catalysts by HRTEM images, the possible reasons include: (1) the rough surface, (2) the VO_x species highly disperse on the surface of CeO_2 as the amorphous phase, and (3) the easy formation of VO_x films stemming from its layer structure.

The surface acidity and basicity of VO_x/CeO_2 catalysts are characterized via temperature-programmed desorption of NH_3 and CO_2, and the results are shown in Fig. 9. The pure CeO_2 displays two evident peaks of CO_2 desorption, one sharp peak at 170 °C corresponds to the weak basic sites, and another shoulder peak with the maximum at about 330 °C associates with medium-strength basicity. However, after VO_x species are supported on the CeO_2, the sharp peak disappears and a broad CO_2 desorption peak between 125 °C and 450 °C is observed, and the broad peak can be deconvolved to two peaks at about 225 °C and 375 °C. The temperature of CO_2 desorption shifts to high temperature, which indicates that VO_x/CeO_2 catalysts possesses more strong basic sites. Additionally, it can be found that the amount of basic sites on pure CeO_2 is significantly greater than that of VO_x/CeO_2 catalysts, and the desorption peak area decreases with the increase of VO_x loadings, which suggests that the basic sites of VO_x/CeO_2 catalysts are ascribed to the CeO_2 and the weak basic sites can be occupied by the VO_x species. NH_3-TPD profiles (Fig. 9 right) show that a broad peak in the range of 125 °C and 450 °C is observed over all samples, with the

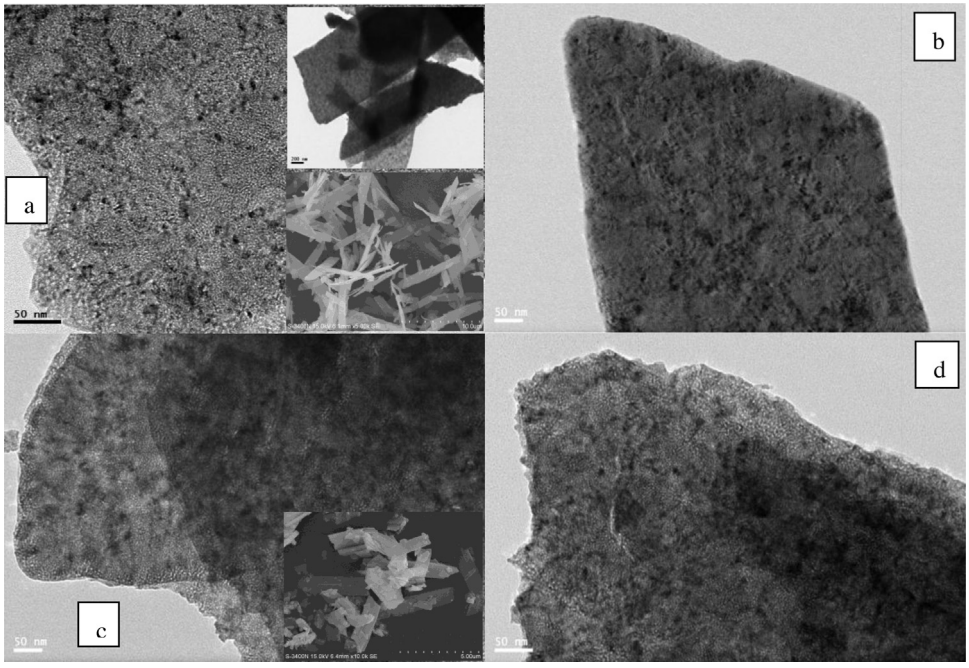

Fig. 8. HRTEM and SEM images of pure CeO_2 (a) $2.5\%VO_x/CeO_2$, (b) $6.0\%VO_x/CeO_2$ (c) and $10\%VO_x/CeO_2$ catalysts (d).

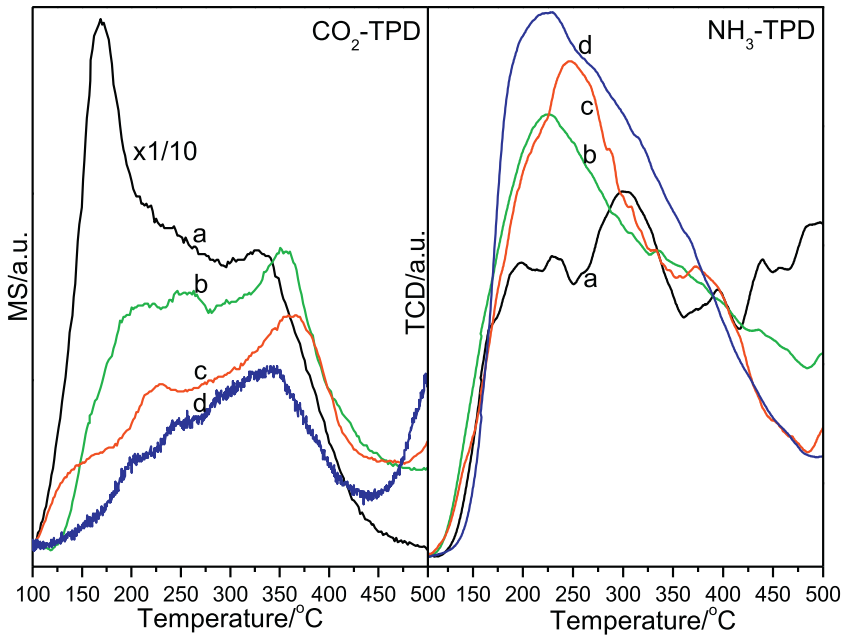

Fig. 9. CO_2-TPD and NH_3-TPD profiles of pure CeO_2 (a) 2.5%VO_x/CeO_2, (b) 6.0%VO_x/CeO_2 (c) and 10%VO_x/CeO_2 catalysts (d).

maximum desorption temperature at about 225–250 °C (for examples, 2.5% and 10%VO_x/CeO_2 catalysts display the maximum desorption at 225 °C, and 6.0%VO_x/CeO_2 shifts to 250 °C), which corresponds to the weak surface acid sites. Moreover, the amount of acid sites increases as loadings of vanadia increased, which indicates that the surface acidity presenting on VO_x/CeO_2 catalysts is mainly from the VO_x species. According to the reports in the literature [23,31], the acid sites existing on pure CeO_2 mainly are assigned to Lewis acid sites, quite a few and weak, while the loading of VO_x can promote obviously both the Lewis and Brönsted acid sites, and the promotion of Brönsted acid sites in quantity is more remarkable due to the presence of the vanadia phase (V^{5+} and V^{4+}) and surface hydroxyl groups bonding vanadium atoms (V—OH).

ESR spectroscopy is a highly sensitive technique for the investigation of VO_x species either in the bulk or at the surface of the catalysts, that reveals useful information about the local structure surrounding the V^{4+} ions. Therefore, the ESR spectra of bulk VO_x and CeO_2 supported VO_x catalysts are shown in Fig. 10. Signal of

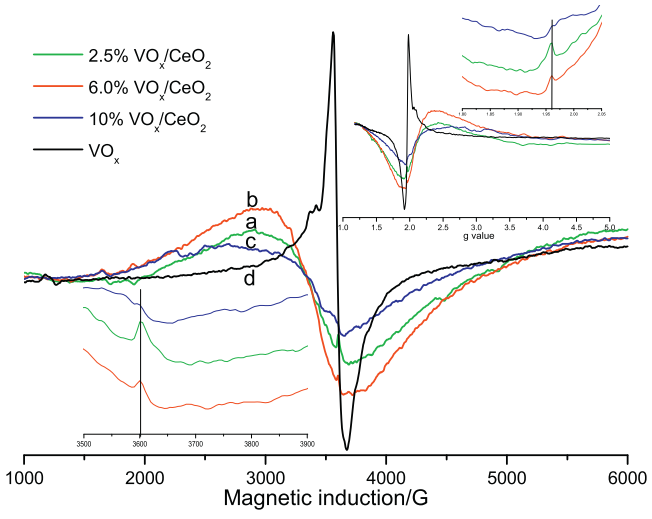

Fig. 10. ESR spectra of 2.5%VO_x/CeO_2 (a) 6.0%VO_x/CeO_2, (b) 10%VO_x/CeO_2 (c) and VO_x catalysts (d).

bulk VO_x (spectrum *d*, Fig. 10) at $g = 1.96$ ($g_{\parallel} = 1.92$, and $g_{\perp} = 1.98$) is sharp and with peak-to-peak line width of 110 G, which is typical for V^{4+} species. The absence of hyperfine structure indicates that the V^{4+} ions are subjected to relatively strong interactions, most likely immersed into a vanadium oxide phase [32]. However, all the VO_x/CeO_2 catalysts exhibit a broad ESR signal, which may be related to the Ce^{3+} ions located in distorted sites of the fluorite lattice [33,34], and the 6.0%VO_x/CeO_2 presents a maximum content of Ce^{3+} according to the signal intensity. Moreover, the *g* values at $g_{\parallel} = 1.93$ and $g_{\perp} = 1.96$ can be obtained for all the VO_x/CeO_2 catalysts, which are attributed to the residual isolated VO^{2+} groups and in good agreement with the reported literature [32]. But it can be found that the g value of VO_x/CeO_2 catalysts are smaller than that of the bulk VO_x, which implies the presence of strong interaction between VO_x and CeO_2, because the values of $g_{\parallel}$ and $g_{\perp}$ depend on the vanadium-ligand distance, increase of $g_{\parallel}$ and $g_{\perp}$ values cause shortening of V—O and V═O bond lengths, respectively [32]. In addition, the signal intensity decreases obviously with the increasing of the VO_x loadings, which indicates that the content of V^{4+} are dropped. The possible reason is that, surface V^{5+} species closely interacting with ceria support can promote a reduction of surface Ce^{4+} to Ce^{3+}, which also suggests that more Ce^{3+}–O^{2-}–V^{5+} sites form on the 6.0%VO_x/CeO_2 catalyst [33].

The valency and atomic ratio of surface V and Ce presented in VO_x/CeO_2 catalysts are investigated by XPS technique and shown in Fig. 11. The binding energies of V $2p_{3/2}$ for 2.5%, 6.0% and 10% VO_x/CeO_2 catalysts decrease slightly with the increase of VO_x loadings are 516.2, 516.1 and 515.7 eV, respectively. Literature data showed that the binding energy for V^{5+} in V_2O_5 was between 517.4 and 516.4 eV, while it was between 515.7 and 515.4 eV for V^{4+} in V_2O_4 [35], which indicates that the coexistence of V^{5+} and V^{4+} species on the surface of VO_x/CeO_2 catalysts and the concentration of V^{4+} species increases with the increase of VO_x loadings, these results are quite different from the bulk phase (ESR results). The XPS spectra of Ce 3d labeled by μ, μ'', ν and ν'' can be correspond to Ce^{4+} species, while μ' and ν'' are assigned to Ce^{3+} species, which confirms the coexistence of Ce^{4+} and Ce^{3+} in all samples. The XPS spectra of O 1s peak can be fitted into two peaks. The peak at lower binding energy (529.5 eV) can be assigned to the lattice oxygen (O_β) and the additional peak at higher binding energy

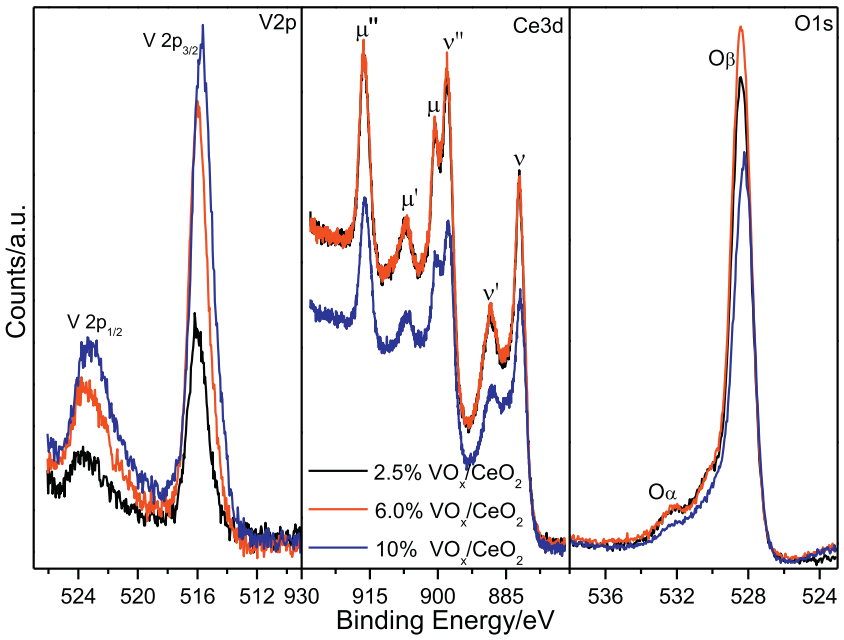

Fig. 11. XPS spectra of V 2p, Ce 3d and O 1s over the VO_x/CeO_2 catalysts.

(532.2 eV) corresponds to the surface chemisorbed oxygen (O_α). Generally, the Oα has been reported to be the most active oxygen in the oxidation reactions due to its higher mobility than the O_β. It can be clearly observed that the percentage of Oα over the surface of 6.0% VO_x/CeO_2 catalyst exhibits a maximum value and the peak intensity of O_β also is the highest. Therefore, the higher catalytic activity of 6.0% VO_x/CeO_2 catalyst for the oxidation of DCE is related to the higher amount of O_α and O_β species. The atomic ratio of surface V and Ce over 2.5%, 6.0% and 10% VO_x/CeO_2 catalysts, V_{surf}/Ce_{surf}, is 0.10, 1.15 and 1.47, respectively. Additionally, the V_{surf}/Ce_{surf} increases with the increase of VO_x loadings and is much higher than the theoretical calculating values (0.048, 0.12 and 0.21), which further ascertains the well dispersion of VO_x on the surface of CeO_2.

3.3. Mechanism study

3.3.1. TPSR and product distribution

The desorption-oxidation behavior of DCE and the formation of products, such as CO_2, CO, HCl and Cl_2, over VO_x/CeO_2 catalysts are further investigated by TPSR technique. Because the sensitivity of the MS is different for each of the compounds shown in Fig. 12, the intensities on the *y*-axis do not correspond to the relative concentration of any compound to another. For instance, the sensitivity of the MS is lower for HCl than chlorine. Nevertheless, an increase (or decrease) in intensity for any compound as a function of temperature represents an increase (or decrease) in concentration of that compound [36]. The spectra for different compounds are obtained simultaneously while rising the reactor temperature

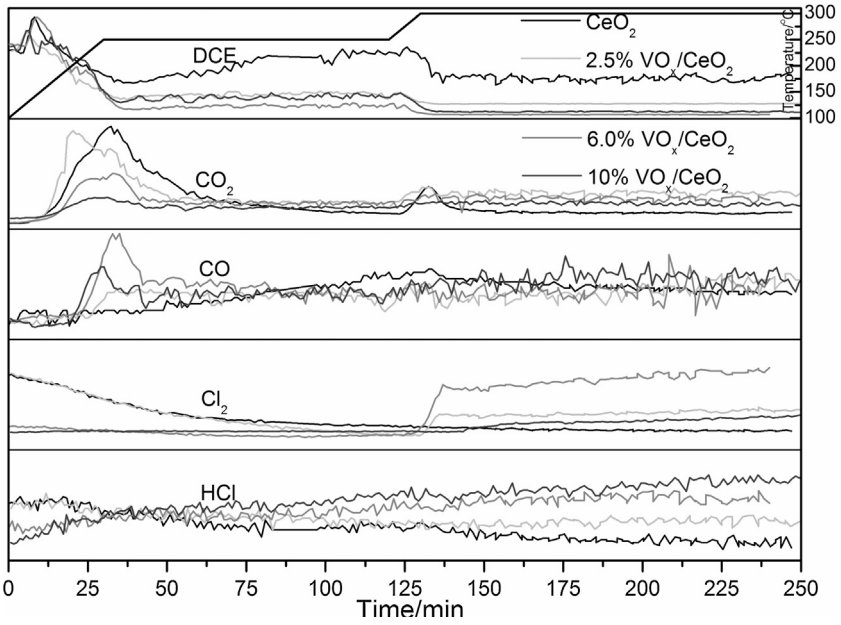

Fig. 12. TPSR profiles for VO_x/CeO_2 catalysts with different VO_x loadings. gas composition: 1000 ppm DCE, 20v/v% O_2, Ar balance; GHSV: 15,000 h^{-1}; catalyst amount: 200 mg.

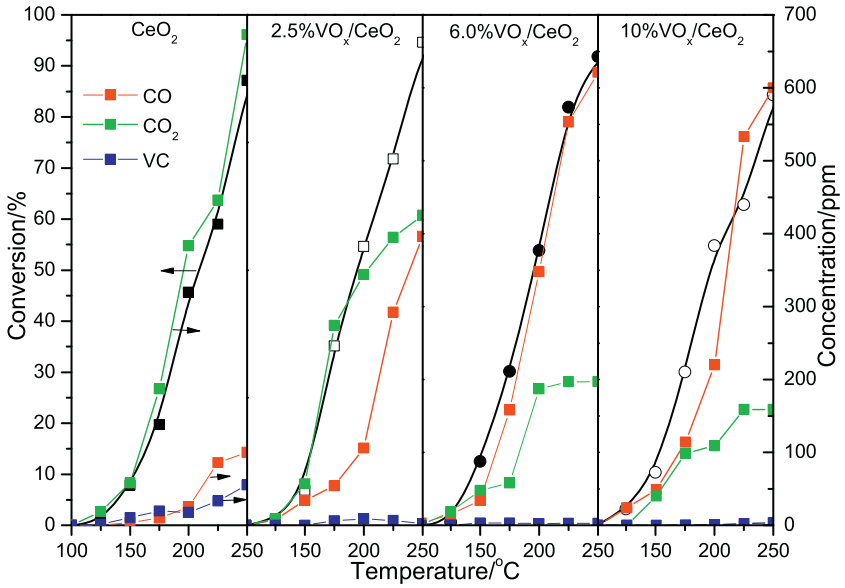

Fig. 13. Distribution of products (CO, CO_2 and VC) over VO_x/CeO_2 catalysts with different VO_x loadings.

via two stages: firstly, from 100 °C to 250 °C at 5 °C/min, and then maintained for 90 min at 250 °C; secondly, from 250 °C to 300 °C at 5 °C/min, and then stayed for 120 min. As presented in Fig. 12, the concentration of DCE increases appreciably with the increasing of reaction temperature over all catalysts, which identifies the presence of the DCE adsorption over CeO_2 based catalysts and the maximum desorption temperature is about 130 °C. Meanwhile, the oxidation of DCE also starts at about 140 °C, which is confirmed by the evolution of CO_2. During the reaction temperature is maintained at 250 °C, the concentration of DCE increases slightly over 2.5% and 10%VO_x/CeO_2 catalysts and rebounds apparently over pure CeO_2, while no measurable increase is observed over 6.0%VO_x/CeO_2. These observations are consistent with the results of the stability tests at 250 °C, namely, the pure CeO_2 catalyst exhibits obvious deactivation and with the loading of VO_x can improve evidently the stability of CeO_2. With the increasing of reaction temperature to 300 °C, the concentration of DCE continues to decrease and the destruction of DCE is complete over VO_x/CeO_2 catalysts. Moreover, the deactivated pure CeO_2 catalyst partially recovers catalytic activity and the conversion of DCE maintains a constant value within 120 min.

The formation of CO_2 and CO over pure CeO_2 and VO_x/CeO_2 catalysts is distinctly different. Almost no CO can be detected over pure CeO_2 (but a small amount of CO is observed after the deactivation of CeO_2 occurs), however, appreciable CO can be observed over VO_x/CeO_2 catalysts and the amount increases with the increasing of VO_x loadings. Additionally, the CO formation occurs at higher temperature compared with CO_2 formation. Generally, the oxygen species adsorbed on oxygen vacancies via the adsorption-activation of gaseous oxygen are considered as the active oxygen species for the total oxidation of CO or other organic compounds, and the previous Raman results also showed that the surface oxygen vacancies of VO_x/CeO_2 catalysts apparently declined due to the loading of VO_x species and decreased with the increasing of VO_x loadings. Therefore, the low selectivity of CO_2 over VO_x/CeO_2 catalysts may be attributed to the less surface oxygen vacancies and low oxidation performance. Furthermore, a small amount of CO formation over the deactivated CeO_2 also can be ascribed to the decrease of active oxygen species, which attributed to the adsorption of inorganic chlorine species on the surface oxygen vacancies.

No hydrogen chloride appears to be formed over all catalysts, which probably because the sensitivity of the MS for hydrogen chloride is low. The formation of HCl over all catalysts is observed by using an HCl gas-detector (Shenzhen Penglei Technology Co., Ltd. PN-M4P), and the HCl concentration is beyond 200 ppm (the detection limit of the above detector) at 250 °C. Moreover, the gaseous Cl_2 in the effluent is not detected at 250 °C. When the reaction temperature increases to 300 °C, the Cl_2 formation is observed over VO_x/CeO_2 catalysts and 6.0%VO_x/CeO_2 exhibits the highest selectivity to Cl_2. However, the appreciable Cl_2 is still not detected over pure CeO_2. For the catalytic combustion of CVOCs, the Cl_2 formation is often associated with the oxidation of HCl (Deacon reaction) or the combination of other inorganic chlorine species (such as dissociatively adsorbed Cl) [37]. Some literature reported that VO_x was investigated as a novel catalytic system for oxidation of hydrogen chloride and showed a better activity in a range of relatively low temperatures (250–350 °C) [38,39]. Hence, the high selectivity of Cl_2 over VO_x/CeO_2 catalysts stems from the good catalytic performance of VO_x species for Deacon reaction. Summarily, VO_x/CeO_2 catalysts present an outstanding activity and stability at low temperature (such as 250 °C), and the main inorganic products containing chlorine is HCl, not Cl_2, which is crucial for the catalytic combustion of CVOCs to avoid the formation of polychlorinated byproducts.

To measure the concentration of products or by-products such as CO_2, VC and CO more accurately, experiments are conducted at steady state and the trends in concentration levels are displayed in Fig. 13. The formation of VC over pure CeO_2 catalyst is obviously observed and the maximum concentration is 50 ppm at 250 °C, however, VO_x/CeO_2 catalysts demonstrate a very low selectivity to VC and the maximum concentration lowers than 5 ppm. Moreover, the amount of VC decreases with the increasing of VO_x loadings and is lower than 2 ppm over 6.0% and 10%VO_x/CeO_2 catalysts. Therefore, the introduction of VO_x species apparently inhibits the formation of VC over CeO_2 based catalyst. Generally, the formation of VC results from the abstraction of HCl (dehydrochlorination), which is considered as the first step for the destruction of DCE and as an intermediate product [40]. However, VC is very stable owing to the low mobility of its chlorine atom (explained by the presence of conjugation effect between the unshared electron pairs of the chlorine atoms and the double bond), thus does not undergo further dehydrochlorination or oxidation to CO, CO_2, H_2O, HCl and Cl_2. The mechanism of HCl abstraction, so-called two-step process, is less likely to occur over CeO_2 based catalysts, and VC should be more

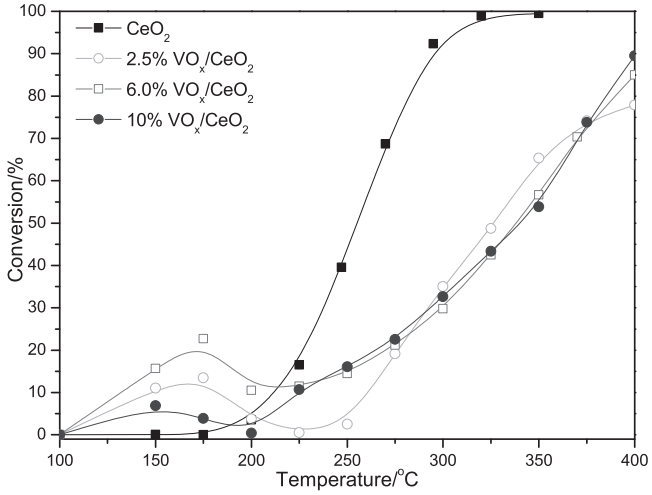

Fig. 14. Light-off curves of vinyl chloride over VO_x/CeO_2 catalysts with different VO_x loadings.

considered as a by-product, not an intermediate product. Therefore, it can be speculated that the basic sites presenting in CeO_2 are responsible for the formation of VC, moreover, the low VC selectivity of VO_x/CeO_2 catalysts is related to the weak base strength and good oxidation performance. Additionally, the distinct difference between CO_2 and CO formation observed in TPSR experiments over pure CeO_2 and VO_x/CeO_2 catalysts is further confirmed. The selectivity to CO_2 over pure CeO_2 catalyst is 85%, while the selectivity to CO over VO_x/CeO_2 catalysts increases with the increasing of VO_x loadings, such as 75% and 79% over 6.0% and 10%VO_x/CeO_2, respectively.

3.3.2. Oxidation of vinyl chloride as byproduct

Considering a large amount of emission with low concentration of vinyl chloride (VC) in the industrial production process for polyvinyl chloride (PVC) and the formation of VC over CeO_2 based catalysts during the catalytic oxidation of DCE, especially over pure CeO_2, the catalytic oxidation of VC over VO_x/CeO_2 catalysts is investigated and the light-off curves are presented in Fig. 14. Compared with DCE, the destruction of VC over VO_x/CeO_2 catalysts is more difficult. The complete oxidation of VC over pure CeO_2 catalyst is only obtained at 300 °C and the T_{90} value over VO_x/CeO_2 catalysts is still not achieved at 400 °C. The bond dissociation energies (BDEs) of C—Cl in vinyl chloride (396.5 ± 4.8 kJ/mol) is higher than that of 1,2-dichloroethane (345.1 ± 5 kJ/mol), which is responsible for the difficult destruction of VC. Besides, these results also verify that the two-step process (HCl abstraction mechanism) is unlikely over CeO_2 based catalysts, which has nevertheless been accepted that the first step in the catalytic decomposition of CVOCs is the splitting of the first Cl atom [40]. Surprisingly, the loading of VO_x conversely inhibits the catalytic destruction of VC over CeO_2 (an exception at low temperature ranges), which is completely different from the catalytic oxidation of DCE and probably because the acid catalysis mechanism of VC destruction over VO_x/CeO_2 catalysts is dominant due to abundant Lewis acid sites (V═O) and Brönsted acid sites (V—O(H)—V) on VO_x species [41] and the presence of C═C double bond in VC molecules. The solid acid catalysts usually present a poor catalytic activity for CVOCs oxidation, especially for CVOCs with stabilized delocalized π bonds due to C═C double bond conjugating with Cl. However, the reasons that VO_x/CeO_2 catalysts exhibit better activity at low temperature ranges are still unknown, which may come from catalysis of the vanadia-ceria interface in VO_x/CeO_2 catalysts or the adsorption of VC on acid sites.

3.3.3. Effect of gaseous and lattice oxygen

Fig. 15 presents the relation between gaseous O_2 and the stability of VO_x/CeO_2 catalysts for DCE catalytic oxidation at 250 °C via two switching loops of gaseous O_2. For the pure CeO_2 catalyst, the rapid deactivation is both observed during the two stages in the presence of gaseous O_2, which is in good agreement with the results of activity tests (Fig. 1). Additionally, after switching from 0%(v/v) O_2 to 20%(v/v) O_2, the conversion of DCE is immediately recovered and then continues to decline. While cutting off oxygen again, the catalytic activity slightly increases instead and can be maintained within 2 h, but the main product is VC. All VO_x/CeO_2 catalysts exhibit a good stability in the presence of oxygen and a slowly declined activity (except 2.5%VO_x/CeO_2) under the oxygen-deprived conditions. Unlike pure CeO_2 catalyst, the catalytic activity of VO_x/CeO_2 catalysts recovers gradually

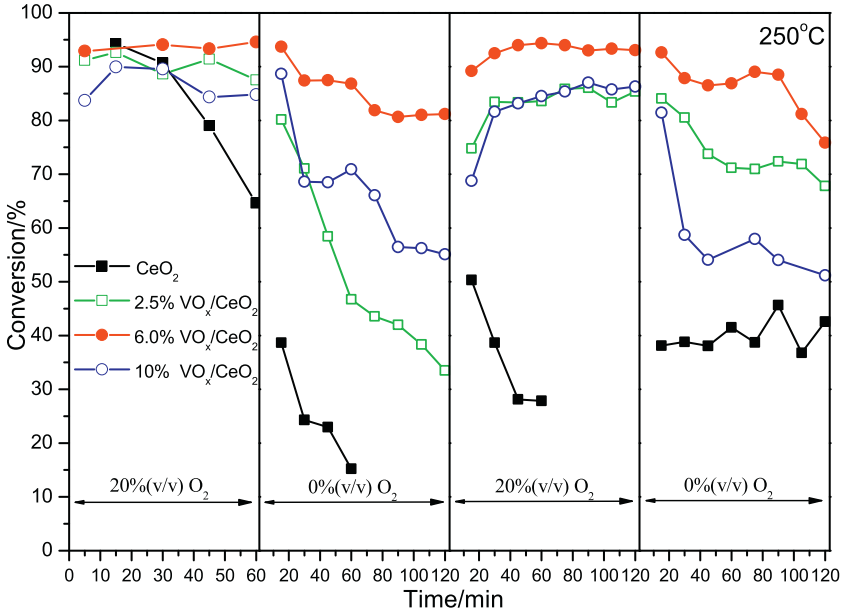

Fig. 15. Effects of gaseous O_2 on the stability of CeO_2 and VO_x/CeO_2 catalysts for DCE catalytic oxidation. gas composition: 450 ppm DCE, 20% or 0% (v/v) O_2, Ar balance; GHSV: 15,000 h^{-1}; catalyst amount: 200 mg; reaction temperature: 250 °C.

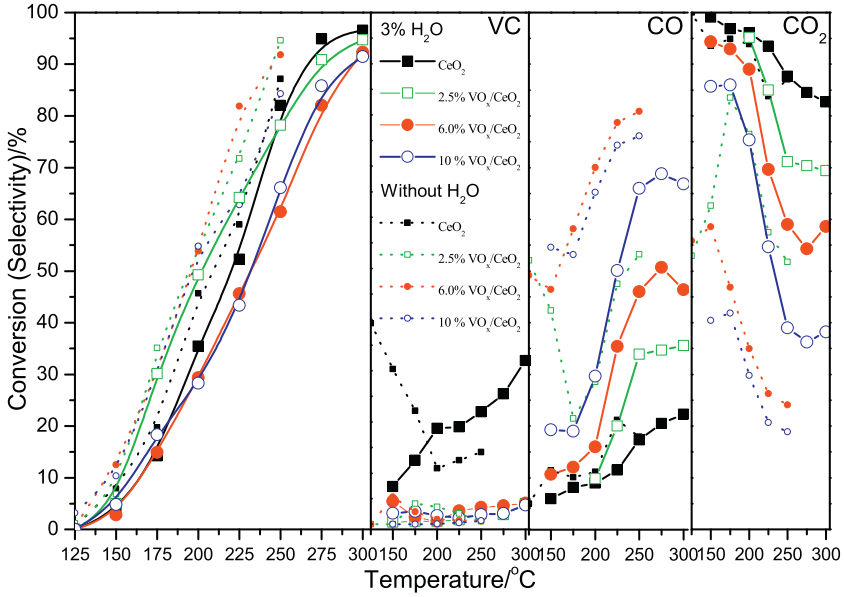

Fig. 16. The light-off curves and selectivity for the catalytic oxidation of DCE over pure CeO_2 and VO_x/CeO_2 catalysts under dry and humid (3v/v% H_2O) conditions.

after the oxygen is switched into the reaction system again. These phenomena, for examples, a high CO selectivity, a slowly declined activity in the absence of oxygen and the gradual recovery of catalytic activity, show that DCE is mainly oxidized by the lattice oxygen species of VO_x over VO_x/CeO_2 catalysts, because the lattice oxygen only displays the poor performance of the complete oxidation and the replenishing of the lattice oxygen is a slow step via the pathway including gaseous oxygen – lattice oxygen of CeO_2 – lattice oxygen of VO_x. While the surface active oxygen species located at oxygen vacancies are responsible for the total oxidation of DCE over pure CeO_2 catalyst, which causes the high CO_2 selectivity. Moreover, the CO selectivity is nearly unchanged over VO_x/CeO_2 catalysts in the presence and absence of oxygen, which also confirms the role of lattice oxygen.

3.3.4. *Effect of water*

The light-off curves and selectivity for the catalytic oxidation of DCE over pure CeO_2 and VO_x/CeO_2 catalysts under dry and humid (3v/v% H_2O) conditions are shown in Fig. 16. With the induction of water in the feed, an obviously negative effect on the performance of VO_x/CeO_2 catalysts can be observed and this allied negative influence on the activity of vanadium oxide based catalysts [42–44] and $Ce_xZr_{1-x}O_2$ mixed oxides [45] had already been reported, generally, which was ascribed to a competitive adsorption between water molecule and chlorinated compounds on active sites. However, it can be found that the inhibiting effect is more perceptible for 6.0%VO_x/CeO_2 and 10%VO_x/CeO_2 (with a higher VO_x loading), and the both exhibit an almost overlapping light-off curve under humid condition. By contrast, the effect of water on the pure CeO_2 catalyst is almost negligible, this slight inhibition reflects the unfavoured adsorption of the chlorinated compounds at the catalytic sites in the presence of water molecules [45]. Therefore, it is considered that the effect of water on the surface acidity of VO_x/CeO_2 catalysts, such as decreasing the number of medium and strong acid sites [45], is probable another important reason except the competitive adsorption. The NH_3-TPD results also indicate that the surface acidity increases with the increasing of VO_x loading, which causes the significant impact on the VO_x/CeO_2 catalysts with a higher VO_x loading.

Additionally, the product distributions observed at different temperatures under dry and humid conditions show that the VC selectivity is enhanced obviously and increases with rising temperature in the presence of water, especially over pure CeO_2 catalysts. The possible reason is that the water increases the number of basic sites because new basic sites are created on the oxygen atom of adsorbed water [46]. Moreover, water also results in a decrease in CO formation, which may be ascribed to the water gas-shift reaction ($CO + H_2O \rightarrow CO_2 + H_2$), thus leading to a significant improvement in CO_2 formation. As well known, CeO_2 as supports or catalysts was widely applied in the low-temperature water-gas shift reaction [47,48], and vanadium also can promote the performance of Pt/CeO_2 catalyst for this reaction due to the presence of the V—O—Ce bonds [49].

3.3.5. *In situ FT-IR studies*

In situ reaction is investigated via FT-IR spectra technique to study the mechanism of DCE oxidation. Fig. 17 displays the DRIFTS spectra of DCE adsorbed on pure CeO_2 and VO_x/CeO_2 catalysts at different temperatures (from 50 to 300 °C) under O_2/N_2 atmosphere. First, some commons and differences can be summarized briefly as follows:

(1) two negative bands in the ranges of 3650 and 3700 cm^{-1}, indicative of disappearing species, are noticed on all catalysts. Moreover, the intensity initially increases and then decrease with the increase of reaction temperature and the maximum value is observed at 200 °C;
(2) all the VO_x/CeO_2 catalysts display four bands at about 2715, 2740, 2804, 2874 and 2960 cm^{-1} and the intensity increases with the increase of reaction temperature, but pure CeO_2 only exhibits negligible weak bands;
(3) between 2000 cm^{-1} and 2400 cm^{-1}, exactly a series of bands at about 2340, 2275, 2170 and 2150 cm^{-1} are observed over all VO_x/CeO_2 catalysts, however, pure CeO_2 only exhibits a band at 2121 cm^{-1};
(4) in the range of 1200–1700 cm^{-1}, some bands located at around 1234, 1283, 1309 and 1426 cm^{-1} are observed on 6.0% and 10%VO_x/CeO_2 catalysts, but no bands are detected on pure CeO_2 and 2.5%VO_x/CeO_2 catalysts.

In the range of OH group vibration, the negative bands in the subtraction spectra at around 3690 and 3660 cm^{-1} for pure CeO_2 and

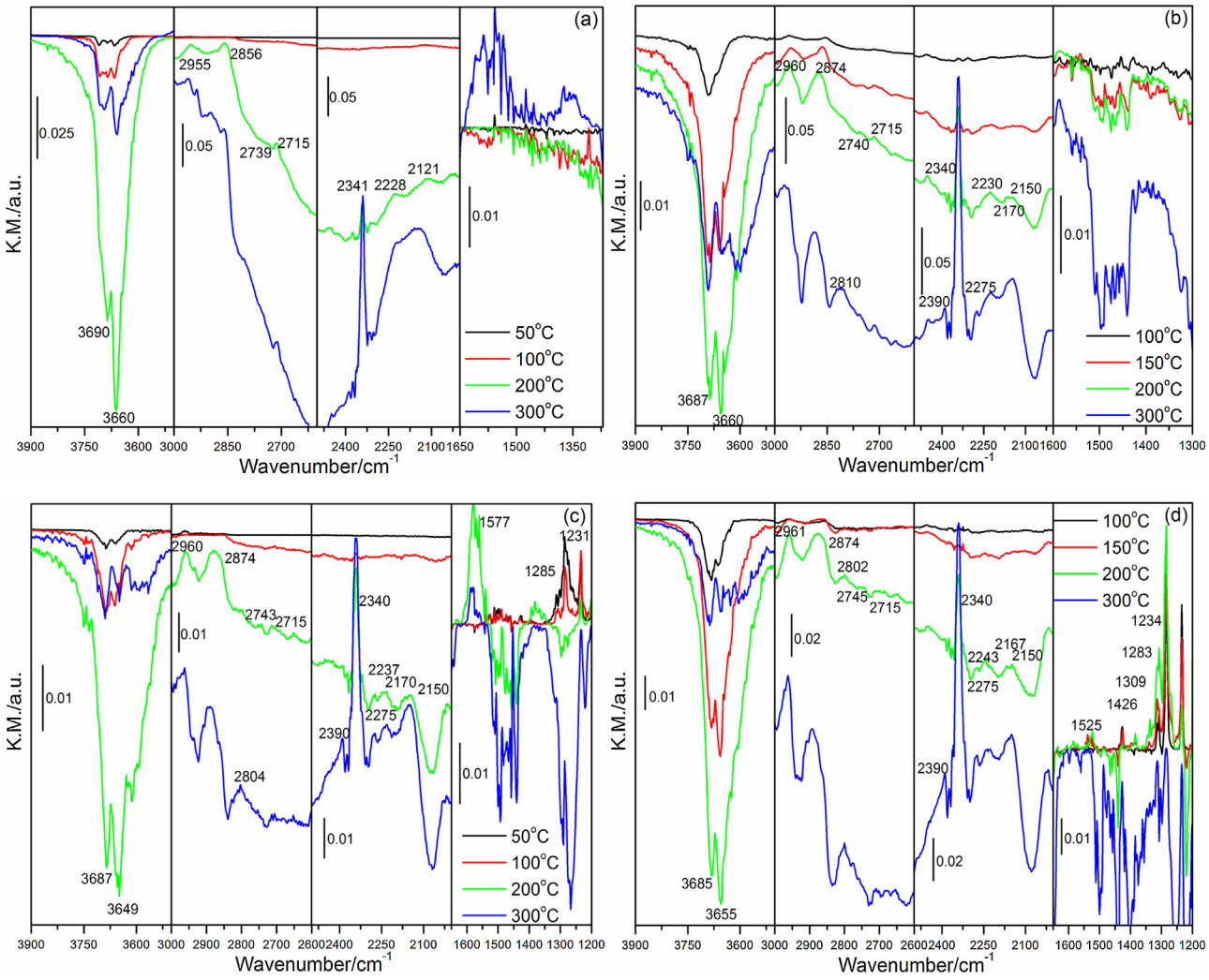

Fig. 17. In situ DRIFTS spectra of DCE adsorbed on pure CeO_2 (a) 2.5%VO_x/CeO_2, (b) 6.0%VO_x/CeO_2, (c) and 10%VO_x/CeO_2 (d) at different temperature.

2.5%VO_x/CeO_2 catalysts, while shift to low wavenumber (3685 and 3655 cm^{-1}) for 6%VO_x/CeO_2 and 10%VO_x/CeO_2 catalysts, should be attributed to the OH vibration mode of hydroxyl groups of CeO_2 and VO_x. The former (3690 and 3685 cm^{-1}) can be assigned to the isolated OH groups on the CeO_2 and VO_x surface, respectively, and the latter (3660 and 3655 cm^{-1}) corresponds to the bridged OH groups. It is obvious that these sites are occupied with DCE by physical adsorption or chemi-adsorbed species. However, DCE adsorption at 50 °C should be considered as molecular, because the intensity decreases sharply with the purging time and no other new bands appear in the low frequency region. Increasing the reaction temperature, the reactive adsorption occurs and the intensity increases rapidly. Importantly, the intensity of negative bands corresponding to hydroxyl groups reduces obviously when the reaction temperature is heated up to 300 °C, whereas activity tests indicate that the complete oxidation of DCE had already occurred, which suggests that the occupied or consumed hydroxyl groups (the H atom in OH can be supplied to the dissociated DCE or reacts with Cl species adsorbed on active sites to form HCl) can be recovered (the H atom in the dissociated DCE can be transferred to O^- and forms OH or the dissociative adsorption of H_2O produced by the oxidation of DCE) after the oxidation of DCE is completed. The recovery of surface hydroxyl groups is very important, which ensures the high selectivity to HCl and stability.

In the range of 1700–1200 cm^{-1}, the catalysts with low VO_x loadings (pure CeO_2 and 2.5%VO_x/CeO_2 catalysts) exhibit different characteristics from that of high VO_x loadings (6.0% and 10%VO_x/CeO_2 catalysts), no obvious bands are observed on the former, while the latter displays a series of sharp bands located at around 1426, 1234, 1283 and 1309 cm^{-1} which may be related to the deformation of —CH_2— and —CH— group, for examples, $\delta(CH_2Cl)$, δ(HCCl), δ(CCH) and ν(CC) + δ(CCH), indicating that DCE can be adsorbed and activated. Moreover, the intensity of these bands decreases with the increase of reaction temperature, suggesting that the oxidation of DCE occurs. Additionally, it can be speculated that the adsorption and activation of DCE mainly performs on CeO_2, and this process is weak and fast when the VO_x loadings are below the monolayer dispersion thresholds. However, for the 6.0% and 10%VO_x/CeO_2 catalysts, the CeO_2 surface is covered by VO_x species, thus, a part of DCE strongly adsorbs on Brönsted acid sites presenting on VO_x species or VO_x–CeO_2 interface.

The weak bands at about 2874 cm^{-1} and 2960 cm^{-1} are assigned to the —CH— stretching vibration, ν(CH), such as CH_2- and CH_3-groups in various compounds, including 1,2-dichloroethane and CH_3CHO and CH_3COOH. Generally, these bands are considered as the absorbed DCE on catalysts surface [50]. However, it can be found that the strength of these bands get stronger as the reaction temperature increases with the exception of pure CeO_2, thus, these

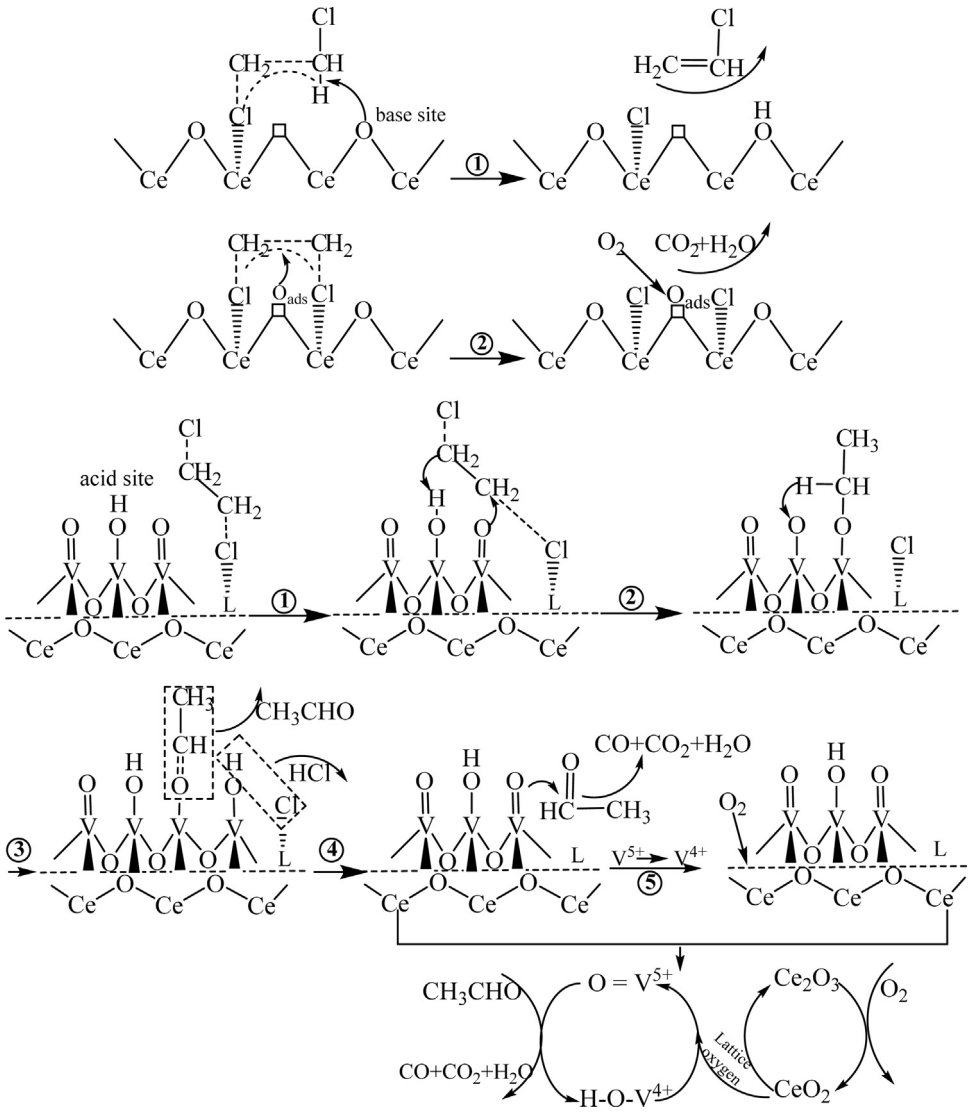

Scheme 1. Proposed reaction mechanisms for the oxidation of 1,2-dichloroethane over pure CeO_2 and VO_x/CeO_2 catalysts.

bands should be irrelevant to the absorbed DCE. Additionally, the doublet bands at about 2740 and 2715 cm^{-1} are attributed to the aldehydic C—H stretch, because the position of the aldehydic C—H stretch in saturated aldehydes is somewhat sensitive to branching on the α carbon. If the α carbon is unbranched (CH_3 or CH_2 group), the aldehydic C—H stretch appears between 2730 and 2715 cm^{-1} [51]. Meanwhile, the band assigning to $\nu s(CH_3)$ at 2804 cm^{-1} also is observed. Therefore, the bands at around 2715, 2740, 2804, 2874 and 2960 cm^{-1} can be identified as the characteristic bands of intermediate products CH_3CHO. Compared with VO_x/CeO_2 catalysts, the intensity of CH_3CHO over pure CeO_2 is evidently weak, especially at higher temperature (300 °C), which is possible for two reasons: (1) the pathway forming intermediate products CH_3CHO is not a main pathway for pure CeO_2 catalyst, (2) the produced CH_3CHO can be oxidized rapidly to CO_x due to the excellent oxidation performance and abundant oxygen vacancies of CeO_2.

The band appeared at about 2340 cm^{-1} which could be ascribed to CO_2 adsorbed on the surface of catalysts [52], and the intensity increases with the increase of reaction temperature. For the VO_x/CeO_2 catalysts, three bands at 2275, 2170 and 2150 cm^{-1} are observed and the intensity also increases with the increase of reaction temperature. Hadjiivanov reported that the adsorption of CO on potassium exchanged EMT zeolite provoked the emergence of three regions: weak broad peak appears at 2275 cm^{-1}, two strong peaks at 2160 and 2147 cm^{-1} and very weak broad peak at 2120 cm^{-1} [53], and Areán suggested that IR spectra of CO adsorbed on K-FER showed the existence of two main peaks located at 2166 and 2150 cm^{-1} [54]. Additionally, Gutiérrez-Ortiz assigned the band at 2155 cm^{-1} to CO linearly adsorbed on surface-exposed metal ions, e.g., Lewis sites [55]. Therefore, these bands on VO_x/CeO_2 catalysts can be attributed to the adsorption of CO on $V^{5+/4+}$. The band observed at 2121 cm^{-1} on pure CeO_2 catalyst is assigned to the adsorption of CO [52].

Additionally, bands corresponding to the vinyl chloride, such as $\nu s(CH_2)$: 3030 cm^{-1}, $\rho(CH)$: 1288 and 1260 cm^{-1}, $\rho(CH_2)$: 1033 cm^{-1}, $\nu(C{=}C)$: 1552 cm^{-1}, $\delta(CH_2)$:1599 cm^{-1}, are not observed, however, it can be clearly seen that vinyl chloride is formed during activity tests (Fig. 13). The rapid desorption and weak absorption of vinyl chloride should be responsible for this phenomenon.

Based on the results achieved in the current work and our previous studies [19,34,37], we propose that the total oxidation of 1,2-dichloroethane over pure CeO_2 and VO_x/CeO_2 catalysts proceeds through a mechanism shown in Scheme 1. The first step of this mechanism is believed to be a dissociative adsorption of C—Cl bonds on Lewis acid sites (such as $Ce^{4+/3+}$ or $V^{5+/4+}$) occurs via Cl

abstraction. For pure CeO_2, the adsorption of DCE mainly includes two ways due to the rotatability of C—C single bond and the presence of various active sites: (1) adsorption of only one Cl on Lewis acid site, and (2) adsorption of two Cl on two Lewis acid sites, respectively. When the dissociative adsorption of DCE occurs via Way (1), the basic site (O^{2-}) nucleophilic attacks another carbon atom and captures one hydrogen atom, and then the by-product VC forms through an E2 elimination reaction. Because VC is very stable, the further dissociation and oxidation are difficult. Additionally, the basicity of CeO_2 is very weak, thus, the higher temperature is favorable to the formation of VC. However, the two Cl simultaneously adsorbs and dissociates on Lewis acid sites, being the main way, and the C—C and C—Cl bonds in DCE are activated. Afterwards, the O_{ads} species on the oxygen vacancies of CeO_2 with the excellent oxidizing ability rapidly oxidize the dissociated DCE to CO_2 and H_2O. Most of Cl species adsorb on active sites and result in the deactivation of CeO_2, moreover, part of Cl species can be removed from CeO_2 surface in the form of HCl via the reaction of surface hydroxy groups and the dissociatively adsorbed Cl, or in the form of Cl_2 at elevated temperature via the Deacon reaction.

For VO_x/CeO_2 catalysts, the dissociation of C—Cl bonds is more drastic and easier due to the presence of more various Lewis acid sites ($V^{5+/4+}$ and $Ce^{4+/3+}$) and Ce^{3+}–O^{2-}–V^{5+} sites, the higher valence and electrophilicity of VO_x species and the possible strong interaction between VO_x and CeO_2 compared with the isolated CeO_2, are responsible for the high catalytic activity. Additionally, the simultaneous adsorption and dissociation of two C—Cl bonds is more dominant due to the absence of abundant basic sites (the lattice oxygen in VO_x species more exhibits the characteristics of the selective oxidation, not basicity). The two activated carbon atoms are subjected to attack by OH groups and lattice oxygen, including the transfer of hydrogen atom and the formation of acetaldehyde intermediate. Namely, the hydrogen in OH is transferred to —CH_2—Cl and the cleavage of Cl—C bond (Cl abstraction) occurs, forming a —CH_3. In our previous work [56], the formation of benzene was observed during catalytic combustion of chlorobenzene over CeO_2 based catalysts, which was thought to be linked to surface hydroxyl groups. Moreover, Xu also reported that the low chlorinated aromatics, such as dichlorobenzene (1,2-, 1,3-, 1,4-), were detected for the catalytic destruction of pentachlorobenzene over V_2O_5–WO_3/TiO_2 catalyst [9]. Meanwhile, a terminal oxygen atom of $[V_2O_5]^+$ directly inserts into the C—Cl bond of another dissociated —CH_2—Cl, and the C—H bond in the dissociated —CH_2—Cl activated. Subsequently, a hydrogen atom is transferred and forms eventually acetaldehyde. Numerous literature pointed that methane, ethane and alcohols can be converted to aldehydes over bulk or supported vanadium oxides through a hydrogen-atom transfer pathway [57–60]. Finally, the acetaldehyde re-adsorbs on catalysts surface, in practice, most of the acetaldehyde species do not desorb from the surface, and can be easily further oxidized to CO_x by the lattice oxygen of V_2O_5. Due to the low total oxidation ability of lattice oxygen, bulk or supported V_2O_5 catalysts generally are considered as a good catalyst for selective oxidation, the main product is CO and the concentration of CO increases with the increase of VO_x loadings. In the process of oxidation, the $V^{5+}O_x$ is reduced to $V^{4+}O_x$ species, and then lattice oxygen of CeO_2 migrates to vanadium in order to reoxidize these $V^{4+}O_x$ species to $V^{5+}O_x$. With the same time, CeO_2 released lattice oxygen can be easily reoxidized by O_2 from the gaseous stream due to its excellent oxygen storage performance.

4. Conclusions

VO_x/CeO_2 catalysts are prepared by a conventional incipient-wetness impregnation method using CeO_2 nanobelts as supports. The monolayer dispersion capacity of VO_x species on CeO_2 nanobelts is determined by several methods, including XRD, Raman, H_2-TPR techniques and activity tests of DCE oxidation. Then, the catalysts of 2.5%VO_x/CeO_2 (the far below monolayer dispersed VO_x), 6.0%VO_x/CeO_2 (the monolayer dispersed VO_x) and 10%VO_x/CeO_2 (the multilayer dispersed VO_x) are characterized detailed by IR, Raman, HRTEM, NH_3-TPD, CO_2-TPD, ESR and XPS and found that the VO_x species are highly dispersed on the surface of CeO_2 nanobelts in the form of amorphous phase, even for 10%VO_x/CeO_2. the loading of VO_x species increases the surface acidity and decreases the surface basicity of CeO_2, and the amount of acid and base is fully dependent on the loadings of VO_x; the V^{5+}/V^{4+} and Ce^{4+}/Ce^{3+} species coexist on the surface and in bulk of VO_x/CeO_2 catalysts. TPSR of DCE and product distribution over VO_x/CeO_2 catalysts with different VO_x loadings suggest that pure CeO_2 can oxidize directly carbon in DCE to CO_2 due to its outstanding total oxidizing ability and abundant active oxygen species adsorbed on oxygen vacancies, however, small amount of by-product VC can be formed due to the presence of weak basic sites. Over VO_x/CeO_2 catalysts, most of the carbon in DCE is partially oxidized to CO, and the selectivity to CO increases with the increase of VO_x loadings, even 79% CO selectivity can be obtained over 10%VO_x/CeO_2 catalysts. High CO selectivity is supposed to relate to the lattice oxygen of VO_x. Finally, a reaction mechanism of DCE total oxidation is proposed over pure CeO_2 and VO_x/CeO_2 catalysts. The first step of this mechanism is believed to be a dissociative adsorption of C—Cl bonds on Lewis acid sites (such as $Ce^{4+/3+}$ or $V^{5+/4+}$) occurs via Cl abstraction. For pure CeO_2 catalysts, the most of dissociated DCE can be oxidized directly and rapidly to CO_2 by surface active oxygen species, but part of activated DCE is attacked by a basic oxygen, which results in the formation of vinyl chloride. Whereas, VO_x/CeO_2 catalysts display a subsequent reaction pathway distinguished from pure CeO_2, and the formation of intermediate acetaldehyde is a key step via C—H bond activation and hydrogen transfer on VO_x species. And then acetaldehyde is further selectively oxidized to CO by the lattice oxygen of VO_x. In the process of oxidation, the $V^{5+}O_x$ is reduced to $V^{4+}O_x$ species, and then lattice oxygen of CeO_2 migrates to vanadium in order to reoxidize these $V^{4+}O_x$ species to $V^{5+}O_x$. Meanwhile, CeO_2 lost lattice oxygen can be easily reoxidized by O_2 from the gaseous stream. Moreover, the Cl species adsorbed on Lewis acid sites can be removed as a form of HCl through reacting with numerous surface hydroxyl groups, which is responsible for the stability of VO_x/CeO_2 catalysts.

VO_x/CeO_2 catalysts present excellent catalytic activity and stability for the total oxidation of DCE, however, a large amount of undesirable partial oxidation product CO is formed. Therefore, improving selectivity to CO_2 is crucial for VO_x/CeO_2 catalysts, and the introduction of transition metals, such as Mn, Ti or Cr, into CeO_2 is desired in order to further enhance the complete oxidation performance and VO_x dispersion.

Acknowledgments

The authors would like to thank Dr. Wei Deng for English language editing. This research was supported by the National Natural Science Foundation of China (Nos. 21307033, 21277047), Shanghai Natural Science Foundation (No. 13ZR1411000), National Basic Research Program of China (Nos. 2010CB732300, 2011AA03A406), Commission of Science and Technology of Shanghai Municipality (No. 11JC1402900), Development Program for Young Teachers in Shanghai Universities and the Opening Project of Key Laboratory of Nuclear Radiation and Nuclear Energy Technology, Chinese Academy of Sciences (NRNE-OP2012001).

References

[1] H. Weber, W. Dimmling, K.H. Moller, Dech. Monog. 80 (1976) 57–76.

[2] M. Kosusko, C.M. Nunez, J. Air Waste Manage. Assoc. 40 (1990) 254–259.
[3] A. Aranzabal, B. Pereda-Ayo, M.P. González-Marcos, J.A. González-Marcos, R. López-Fonseca, J.R. González-Velasco, Chem. Pap. 68 (2014) 1169–1186.
[4] J. Lichtenberger, M.D. Amiridis, J. Catal. 223 (2004) 296–308.
[5] C.E. Hetrick, J. Lichtenberger, M.D. Amiridis, Appl. Catal. B 77 (2008) 255–263.
[6] C.E. Hetrick, F. Patcas, M.D. Amiridis, Appl. Catal. B 101 (2011) 622–628.
[7] E. Finocchio, G. Busca, M. Notaro, Appl. Catal. B 62 (2006) 12–20.
[8] Y. Yang, G. Yu, S.B. Deng, S.W. Wang, Z.Z. Xu, J. Huang, B. Wang, Chem. Eng. J. 192 (2012) 284–291.
[9] Z.Z. Xu, S.B. Deng, Y. Yang, T.T. Zhang, Q.M. Cao, J. Huang, G. Yu, Chemosphere 87 (2012) 1032–1038.
[10] R. Delaigle, D.P. Debecker, F. Bertinchamps, E.M. Gaigneaux, Top. Catal. 52 (2009) 501–516.
[11] F. Elisabetta, R. Gianguido, B. Guido, Catal. Today 169 (2011) 3–9.
[12] A. Stefania, B. Sonia, B. Rosa, Appl. Catal. A 341 (2008) 18–25.
[13] D.P. Debecker, F. Bertinchamps, N. Blangenois, Appl. Catal. B 74 (2007) 223–232.
[14] S. Albonetti, S. Blasioli, A. Bruno, Appl. Catal. B 64 (2006) 1–8.
[15] A.M. Nie, H.S. Yang, Q. Li, Ind. Eng. Chem. Res. 50 (2011) 9944–9948.
[16] B.G. Xie, G.Z. Lu, Q. Dai, Y.Q. Wang, Y.L. Guo, Y. Guo, J. Cluster Sci. 22 (2011) 555–561.
[17] Y.J. Guan, C. Li, Chin. J. Catal. 28 (2007) 392–394.
[18] P. Satu, N. Tuomas, M. Lenka, Appl. Catal. B 138–139 (2013) 33–42.
[19] Q.G. Dai, X.Y. Wang, G.Z. Lu, Appl. Catal. B 81 (2008) 192–202.
[20] B. de Rivas, N. Guillén-Hurtado, R. López-Fonseca, F. Coloma-Pascual, A. García-García, J.I. Gutiérrez-Ortiz, A. Bueno-López, Appl. Catal. B 121–122 (2012) 162–170.
[21] Q.Q. Huang, X.M. Xue, R.X. Zhou, J. Mol. Catal. A 344 (2011) 74–82.
[22] B. de Rivas, R. López-Fonseca, M.Á. Gutiérrez-Ortiz, J.I. Gutiérrez-Ortiz, Appl. Catal. B 101 (2011) 317–325.
[23] Q.G. Dai, S.X. Bai, H. Li, W. Liu, X.Y. Wang, G.Z. Lu, CrystEngComm 16 (2014) 9817–9827.
[24] Y. Peng, C.Z. Wang, J.H. Li, Appl. Catal. B 144 (2014) 538–546.
[25] S.H. Lee, H.M. Cheong, M. Je Seong, P. Liu, C.E. Tracy, A. Mascarenhas, J.R. Pitts, S.K. De, Solid State Ionics 165 (2003) 111–116.
[26] D. Vernardou, E. Spanakis, G. Kenanakis, E. Koudoumas, N. Katsarakisa, Mater. Chem. Phys. 124 (2010) 319–322.
[27] Y.H. Kim, H.I. Lee, Bull. Korean Chem. Soc. 20 (1999) 1457–1463.
[28] Y.C. Xie, Y.Q. Tang, Adv. Catal. 37 (1990) 1–43.
[29] D.A. Bulushev, L. Kiwi-Minsker, V.I. Zaikovskii, A. Renken, J. Catal. 193 (2000) 145–153.
[30] J.R. Sohn, J.B. Park, H.W. Kim, Y.I.I. Pae, Korean J. Chem. Eng. 20 (2003) 48–57.
[31] X.D. Gu, J.Z. Ge, H.L. Zhang, A. Auroux, J.Y. Shen, Thermochim. Acta 451 (2006) 84–93.
[32] K.V. Narayana, B. David Raju, S. Khaja Masthan, V. Venkat Rao, P. Kanta Rao, R. Subrahmanian, A. Martin, Catal. Commun. 5 (2004) 457–462.
[33] M.V. Martínez-Huerta, J.M. Coronado, M. Fernández-García, A. Iglesias-Juez, G. Deo, J.L.G. Fierro, M.A. Bañares, J. Catal. 225 (2004) 240–248.
[34] Q.G. Dai, X.Y. Wang, G.P. Chen, Y. Zheng, G.Z. Lu, Microporous Mesoporous Mater. 100 (2007) 268–275.
[35] V.I. Bukhtiyarov, Catal. Today 56 (2000) 403–414.
[36] K. Ramnathan, J.J. Spivey, Combust. Sci. Technol. 63 (1989) 247–255.
[37] Q.G. Dai, S.X. Bai, Z.Y. Wang, X.Y. Wang, G.Z. Lu, Appl. Catal. B 126 (2012) 64–75.
[38] V.E. Tarabanko, N.V. Tarabanko, A.M. Zhyzhaev, N.V. Koropachinskaya, Sib FU. Chem. 2 (2009) 11–18.
[39] Hisham, S.W. Benson, J. Phys. Chem. 99 (1995) 6194–6198.
[40] B. Ramachandran, H.L. Greene, S. Chatterjee, Appl. Catal. B 8 (1996) 157–182.
[41] F.S. Tang, K. Zhuang, F. Yang, L.L. Yang, B.L. Xu, J.H. Qiu, Y.N. Fan, Chin. J. Catal. 33 (2012) 933–940.
[42] M. Stoll, J. Furrer, H. Seifert, G. Schaub, D. Unruh, Waste Manage. 21 (2001) 457–463.
[43] S. Krishnamoorthy, J.A. Rivas, M.D. Amiridis, J. Catal. 193 (2000) 264–272.
[44] J. Jones, J.R.H. Ross, Catal. Today 35 (1997) 97–105.
[45] B. de Rivas, R. López-Fonseca, M.A. Gutiérrez-Ortiz, J.I. Gutiérrez-Ortiz, Chemosphere 75 (2009) 1356–1362.
[46] M. Isao, U. Atsuko, F. Hiroshi, T. Kenjiro, J. Catal. 51 (1978) 72–79.
[47] A. Luengnaruemitchai, S. Osuwan, E. Gulari, Catal. Commun. 4 (2003) 215–221.
[48] D. Andreeva, V. Idakiev, T. Tabakova, L. Ilieva, P. Falaras, A. Bourlinos, A. Travlos, Catal. Today 72 (2002) 51–57.
[49] A.M. Duarte de Farias, P. Bargiela, da G.C. Rocha, M.A. Fraga, J. Catal. 260 (2008) 93–102.
[50] P. Yang, Z.H. Meng, S.S. Yang, Z.N. Shi, R.X. Zhou, J. Mol. Catal. A 393 (2014) 75–83.
[51] B.C. Smith, Infrared Spectral Interpretation: A Systematic Approach, CRC Press, 1998, 2014, pp. 98.
[52] X.Y. Liu, A.Q. Wang, L. Li, T. Zhang, C.Y. Mou, J.F. Lee, J. Catal. 278 (2011) 288–296.
[53] K. Hadjiivanov, P. Massiani, H. Knözinger, Phys. Chem. Chem. Phys. 1 (1999) 3831–3838.
[54] C.O. Areán, D. Nachtigallová, P. Nachtigall, E. Garrone, M.R. Delgado, Phys. Chem. Chem. Phys. 9 (2007) 1421–1437.
[55] B. de Rivas, C. Sampedro, E.V. Ramos-Fernández, R. López-Fonseca, J. Gascon, M. Makkee, J.I. Gutiérrez-Ortiz, Appl. Catal. A 456 (2013) 96–104.
[56] Q.G. Dai, S.X. Bai, X.Y. Wang, G.Z. Lu, Appl. Catal. B 129 (2013) 580–588.
[57] X.N. Wu, S.Y. Tang, H.T. Zhao, T. Weiske, M. Schlangen, H. Schwarz, Chem. Eur. J. 20 (2014) 6672–6677.
[58] K. Wada, H. Yamada, Y. Watanabe, T. Mitsudo, J. Chem. Soc. Faraday Trans. 94 (1998) 1771–1778.
[59] H. Launay, S. Loridant, D.L. Nguyen, A.M. Volodin, J.L. Dubois, J.M.M. Millet, Catal. Today 128 (2007) 176–182.
[60] G.L. Dai, Z.H. Li, W.N. Wang, J. Liu, K.N. Fan, Chin. J. Catal. 34 (2013) 906–910.